JOURNAL OF APPLIED CRYSTALLOGRAPHY

ISSN 1600-5767

Elastic behaviour of orientation-correlated grains in multiphase aggregates

Thomas Gnäupel-Herold*

Center for Neutron Research, National Institute of Standards and Technology, 100 Bureau Drive, Stop 6102, Gaithersburg, MD 20899-6102, USA. *Correspondence e-mail: tg-h@nist.gov

Received 26 May 2023
Accepted 21 September 2023

Edited by T. J. Sato, Tohoku University, Japan

Keywords: diffraction; elastic constants; polycrystals; single crystals; stress; strain; multiphase.

Diffraction elastic constants (DECs) describe the elastic response of a subset of orientation-correlated grains which share a common lattice vector. DECs reflect the elastic behaviour of the single-crystal constituents through their dependence on grain orientation. DECs furthermore depend on the behaviour of the polycrystal aggregate both through the dependence on preferred orientation and through the average elastic interaction of the grains in the subset with their surroundings. The latter is also known as grain–matrix interaction which is grain-shape dependent. Both dependencies can make the DECs uniquely sensitive to the elastic effects of the grain shape, texture and phase composition. Several micro-mechanical models are explored for use in calculating both DECs and overall elastic constants. Furthermore, it is shown how discrete data from electron backscatter diffraction on grain shape, grain orientations and neighbouring grains can be used for DEC calculations. Lastly, the inverse problem of calculating single-crystal elastic constants from DECs is discussed in detail. All calculations discussed in this work can be verified using the freely available computer program *IsoDEC*.

1. Introduction

The intent of this work is to provide a detailed framework for the calculations of elastic properties of orientation-correlated subsets of grains in polycrystalline aggregates. Such properties can be measured by diffraction, and the associated elastic constants are known elsewhere as diffraction elastic constants (DECs). DECs relate lattice strain to macroscopic stress for specific, or correlated, grain orientations with a common lattice plane normal. The directionality applies to both the crystal direction of reflecting grains and the sample orientation, which causes DECs to be sensitive to the single-crystal elastic constants, preferred orientation and bulk constants (overall elastic constants of the aggregate), with additional effects stemming from the grain shape. The sensitivity of the DECs to the aforementioned factors depends on the magnitude of the elastic anisotropy of constituent crystallites, which makes DECs an excellent tool for the study of elastic interactions and model evaluation.

The earliest formulation of a DEC model (Möller & Martin, 1939) was based on Reuss' assumption of uniform stress in all grains (Reuss, 1929). The Reuss model represents a lower bound on the bulk elastic stiffnesses where grains do not interact elastically, and DECs are arithmetic averages of single-crystal compliances about the lattice vector that is perpendicular to the reflecting lattice plane, usually denoted by its Miller indices (*hkl*). The absence of the mediating effect of grain interaction leads to poor agreement with

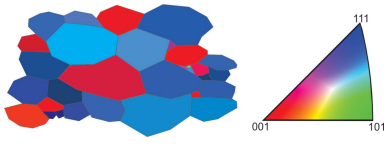

experimental observations in elastic extremum directions; examples are the [100] and [111] directions for grains with cubic crystal symmetry.

Voigt's earlier assumption of homogeneous strain in all grains (Voigt, 1928) represents the upper limit of the overall elastic stiffnesses. It is of limited use for DEC calculations due to the independence with respect to grain orientation. Independence with respect to (*hkl*) contradicts experimental evidence even for moderately anisotropic materials. Hill (1952) suggested the arithmetic average of the Reuss and Voigt limits, which leads to broadly improved agreement with experimental observations both for overall elastic constants and for DECs.

Eshelby's calculation (Eshelby, 1957) of the elastic field of an ellipsoidal inclusion allowed Kröner (1958) to formulate the two bounds of the self-consistent model for the calculation of isotropic overall elastic constants. Kinoshita & Mura (1971), Lin & Mura (1973) and Mura (1987) later developed formulas for the general anisotropic case. One of the Kröner bounds was used for DEC calculations first by Bollenrath *et al.* (1967) for cubic materials, and later by Behnken & Hauck (1986) for all crystal symmetries. DEC calculations using the second Kröner bound were first presented by Gnäupel-Herold *et al.* (2012) where the second bound was referred to as the inverse Kröner model. It was shown that considerable differences between the two bounds exist in DECs due to the opposite responses to the grain shape, particularly in the case of texture. The Kröner bounds in overall elastic constants were frequently examined (Kneer, 1965; Morris, 1970; Walpole, 1969; Willis, 1977), often with particular focus on special cases that allow the formulation of closed expressions. Kneer studied spherical grains, in which case the two bounds coincide. The use of the inverse Kröner model for overall elastic constant calculation has not been widely investigated yet; however, this work shows that aligned ellipsoidal grains produce diverging results for the two bounds in the case of texture or multiphase aggregates. Another unexplored application of Kröner-type models is the direct use of discrete grain orientations and grain shape obtained from electron backscatter diffraction data. Such data allow the computation of individual grain–matrix interactions where certain grain orientations are preferentially surrounded by grains of correlated orientations such as twins, coherent precipitates and martensite. Here, the term 'matrix' is used for grains directly surrounding the crystallite for which the Eshelby tensor is calculated, thus implying that the elastic response of the grain in the centre is different compared with uncorrelated neighbours.

The upper/lower bound nature of elastic constant estimates is rooted in the fact that orientation averages of single-crystal stiffnesses and compliances generally lead to different results. The use of the geometric average proposed by Matthies *et al.* (2001) avoids this issue, thus allowing a single solution and the interchangeable use of compliances and stiffnesses in the partial (DECs) or complete (overall elastic constants) orientation average. For DEC calculations some measure of grain–matrix interaction is included but without considering grain-shape effects. Elastic constants calculated using the geometric average are close in value to the Hill average.

In contrast to overall elastic constants, the DECs retain some dependence on crystal direction through their dependence on the Miller indices (*hkl*). This has been utilized in the formulation of the inverse problem in which the single-crystal elastic constants (SCECs) are calculated from measured DECs (Gnäupel-Herold *et al.*, 1998; Howard & Kisi, 1999; Matthies *et al.*, 2001; Heldmann *et al.*, 2019; Wang *et al.*, 2016). The method presents a viable way to determine alloy SCECs for which large single crystals cannot be produced; however, its scope and limitations have not been explored in depth yet.

2. Modelling

2.1. Numerical approach

2.1.1. Tensor reduction. The need to calculate tensor rotations and the inverse of fourth-rank tensors is commonplace for all models discussed in the following. Moreover, the geometric average discussed later requires the calculation of matrix logarithms and matrix exponentials, both of which can be obtained through Jacobi diagonalization of matrices. The efficient reduction of a fourth-rank tensor with a maximum of 21 independent elements to a symmetric 6×6 matrix described by Matthies & Humbert (1995) and Matthies *et al.* (2001) allows the use of matrix inversion methods as well as significant increases in computational speed. Stiffness and compliance tensors have the twice-symmetric property

$$a_{ijkl} = a_{jikl} = a_{klij}. \tag{1}$$

The dependence of the tensor $a_{ijkl}(g)$ on its orientation is expressed through the orientation matrix g,

$$a_{ijkl}(g) = g^{-1}_{im} g^{-1}_{jn} g^{-1}_{ko} g^{-1}_{lp} a^{(0)}_{mnop},$$
$$i, j, k, l, m, n, o, p = 1 \ldots 3. \tag{2}$$

Here, g_{ij} are components of the rotation matrix g which relates the grain orientation to the sample coordinate system K_A and $a^{(0)}_{mnop}$ refers to the tensor in its principal axis representation, which is tied to the crystallite's unit cell (see Fig. 1). The superscript '−1' for tensors and matrices denotes the inverse quantity. The rotations of tensors and matrices considered in

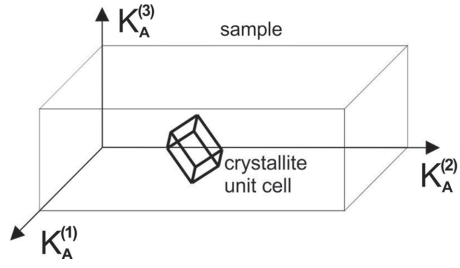

Figure 1
A crystallite in the sample coordinate system.

the following are defined using the coordinate system relationships shown in Fig. 2.

The rotation matrix g transforming $K_B \rightarrow K_A$ is given in Bunge notation (Bunge, 1982) as

$$g(\varphi_1, \Phi, \varphi_2) = \begin{pmatrix} \cos\varphi_1 \cos\varphi_2 & \sin\varphi_1 \cos\varphi_2 & \sin\varphi_2 \sin\Phi \\ -\sin\varphi_1 \sin\varphi_2 \cos\Phi & +\cos\varphi_1 \sin\varphi_2 \cos\Phi & \\ -\cos\varphi_1 \sin\varphi_2 & -\sin\varphi_1 \sin\varphi_2 & \cos\varphi_2 \sin\Phi \\ -\sin\varphi_1 \cos\varphi_2 \cos\Phi & +\cos\varphi_1 \cos\varphi_2 \cos\Phi & \\ \sin\varphi_1 \sin\Phi & -\cos\varphi_1 \sin\Phi & \cos\Phi \end{pmatrix}. \quad (3)$$

$(\varphi_1, \Phi, \varphi_2)$ are Euler angles which are defined by three successive rotations of the orthonormalized crystal frame K_B (initially aligned with K_A). First, K_B is rotated about $K_A^{(3)}$ (Z axis, normal direction – ND) by the angle φ_1. The second rotation Φ occurs about the X axis of the rotated frame ([100] crystal direction, $K_B^{(1)}$) and the third rotation φ_2 is performed about the Z axis of the rotated frame ([001] crystal direction, $K_B^{(3)}$). The successive multiplication of the three rotation matrices leads to (3). Detailed expressions can be found in chapter 1 of the textbook by Bunge (1982) which is available in the public domain.

(1) enables the Voigt matrix notation with a contraction of indices for a symmetric 9×9 scheme:

$$\begin{aligned} &a_{ijkl} \leftrightarrow A_{IJ}^{\mathrm{V}}; \quad ij \leftrightarrow I; \quad kl \leftrightarrow J; \\ &I, J = 1 \ldots 9;\ (11 \leftrightarrow 1), (22 \leftrightarrow 2), (33 \leftrightarrow 3), (23 \leftrightarrow 4), \\ &(31 \leftrightarrow 5), (12 \leftrightarrow 6), (32 \leftrightarrow 7), (13 \leftrightarrow 8) \text{ and } (21 \leftrightarrow 9). \end{aligned} \quad (4)$$

The transformation (4) is followed by the T transformation (Matthies *et al.*, 2001; Matthies & Humbert, 1995) as the double multiplication of the 9×9 matrix A^{V} with the orthogonal matrix T (with the additional property $T = T^{-1}$):

$$T = \begin{pmatrix} 1 & 0 & 0 & 0 & 0 & 0 & 0 & 0 & 0 \\ 0 & 1 & 0 & 0 & 0 & 0 & 0 & 0 & 0 \\ 0 & 0 & 1 & 0 & 0 & 0 & 0 & 0 & 0 \\ 0 & 0 & 0 & \sqrt{\frac{1}{2}} & 0 & 0 & \sqrt{\frac{1}{2}} & 0 & 0 \\ 0 & 0 & 0 & 0 & \sqrt{\frac{1}{2}} & 0 & 0 & \sqrt{\frac{1}{2}} & 0 \\ 0 & 0 & 0 & 0 & 0 & \sqrt{\frac{1}{2}} & 0 & 0 & \sqrt{\frac{1}{2}} \\ 0 & 0 & 0 & \sqrt{\frac{1}{2}} & 0 & 0 & -\sqrt{\frac{1}{2}} & 0 & 0 \\ 0 & 0 & 0 & 0 & \sqrt{\frac{1}{2}} & 0 & 0 & -\sqrt{\frac{1}{2}} & 0 \\ 0 & 0 & 0 & 0 & 0 & \sqrt{\frac{1}{2}} & 0 & 0 & -\sqrt{\frac{1}{2}} \end{pmatrix}. \quad (5)$$

The result of (5) is a symmetric 9×9 matrix where the only non-zero elements are in the upper 6×6 block with $I, J = 1 \ldots 6$, now written as the symmetric matrix A_{IJ} with $I, J = 1 \ldots 6$. Note that because $T = T^{-1}$ forward and backward T transformations are identical. The thus-reduced single-crystal stiffness tensor $c \rightarrow C^{\mathrm{r}}$ and compliance tensor $s \rightarrow S^{\mathrm{r}}$ fulfil the condition

$$C^{\mathrm{r}} = (S^{\mathrm{r}})^{-1}. \quad (6)$$

The tensor rotation in equation (2) is replaced by

$$A_{IJ}(g) = W(g)_{IK} W(g)_{JL} A_{KL}, \quad I, J, K, L = 1 \ldots 6. \quad (7)$$

A_{KL} is the principal axis representation. Equation (7) is derived by Matthies *et al.* (2001). $A_{jk}^{(0)}$ are the components of a matrix-transformed stiffness or compliance tensor in principal axis representation. The matrix $W(g)$ with the property $W(g)^{-1} = W(g^{-1})$ is obtained from the rotation matrix components g_{ij} [explicitly given in equation (3)] and T transformed, leading to the expression

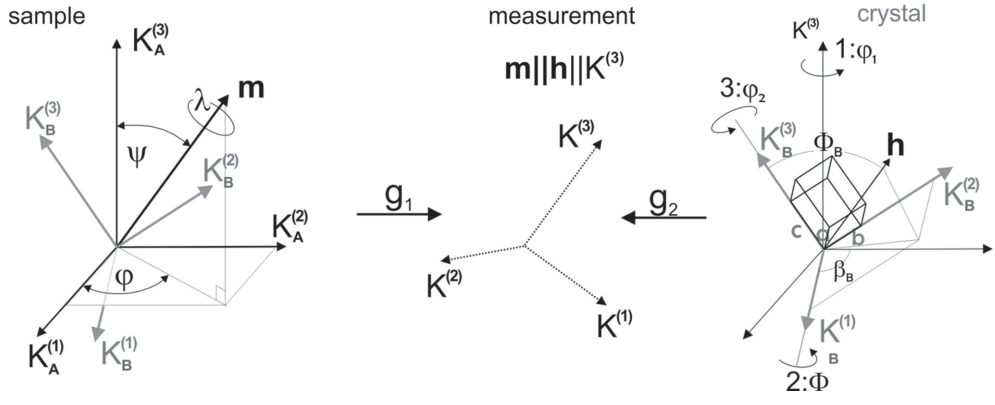

Figure 2
Coordinate systems with angle conventions used in this work. K_A is aligned with the principal directions of the sample; K is the laboratory or measurement system for which the z direction $K^{(3)}$ is parallel to both the measurement direction **m** and the crystal direction **h**. K_B is the orthonormal system attached to the crystal unit cell. The rotation g_1 transforms K_A into K, and g_2 transforms K_B into K. On the right side the Euler angles $(\varphi_1, \Phi, \varphi_2)$ with their respective rotation axes and order of rotations are indicated.

$$W(g) = \begin{pmatrix} g_{11}g_{11} & g_{21}g_{21} & g_{31}g_{31} & \sqrt{2}g_{21}g_{31} & \sqrt{2}g_{11}g_{31} & \sqrt{2}g_{11}g_{21} \\ g_{12}g_{12} & g_{22}g_{22} & g_{32}g_{32} & \sqrt{2}g_{22}g_{32} & \sqrt{2}g_{12}g_{32} & \sqrt{2}g_{12}g_{22} \\ g_{13}g_{13} & g_{23}g_{23} & g_{33}g_{33} & \sqrt{2}g_{23}g_{33} & \sqrt{2}g_{13}g_{33} & \sqrt{2}g_{13}g_{23} \\ \sqrt{2}g_{12}g_{13} & \sqrt{2}g_{22}g_{23} & \sqrt{2}g_{32}g_{33} & g_{22}g_{33} + g_{23}g_{32} & g_{13}g_{32} + g_{12}g_{33} & g_{12}g_{23} + g_{13}g_{22} \\ \sqrt{2}g_{11}g_{13} & \sqrt{2}g_{21}g_{23} & \sqrt{2}g_{31}g_{33} & g_{23}g_{31} + g_{21}g_{33} & g_{11}g_{33} + g_{13}g_{31} & g_{13}g_{21} + g_{11}g_{23} \\ \sqrt{2}g_{11}g_{12} & \sqrt{2}g_{21}g_{22} & \sqrt{2}g_{31}g_{32} & g_{21}g_{32} + g_{22}g_{31} & g_{12}g_{31} + g_{11}g_{32} & g_{11}g_{22} + g_{12}g_{21} \end{pmatrix}. \quad (8)$$

The rotation in equation (7) requires 36^2 floating-point operations compared with 3^8 in equation (2), which is beneficial for the many subsequent cases where the rotation (7) has to be performed multiple times.

Using Euler angles in Bunge notation (Bunge, 1982), the average over all orientations is

$$\overline{A_{IJ}} = \frac{\int A_{IJ}^{(g)} f(g)\,\mathrm{d}g}{\int f(g)\,\mathrm{d}g} = \frac{1}{8\pi^2}\int_0^{\pi}\sin\Phi\,\mathrm{d}\Phi\int_0^{2\pi}\mathrm{d}\varphi_1\int_0^{\pi}\mathrm{d}\varphi_2 W(g)_{IK}W(g)_{JL} \times A_{KL}f(g)\int_0^{\pi}\sin\Phi\,\mathrm{d}\Phi\int_0^{2\pi}\mathrm{d}\varphi_1\int_0^{\pi}\mathrm{d}\varphi_2 f(g) = \frac{1}{8\pi^2}. \quad (9)$$

The matrix elements A_{KL} are placeholders for single-crystal compliances or stiffnesses. $f(g)$ is the value of the orientation distribution function at (φ_1, Φ, φ_2). Equation (9) allows the separate calculation of the orientation average without multiplying A_{KL} for every orientation,

$$\bar{\Omega}_{IJKL} = \frac{1}{8\pi^2}\int_0^{\pi}\sin\Phi\,\mathrm{d}\Phi\int_0^{2\pi}\mathrm{d}\varphi_1\int_0^{\pi}\mathrm{d}\varphi_2 W(g)_{IK}W(g)_{JL}f(g),$$
$$I, J, K, L = 1\ldots6. \quad (10)$$

The matrix Ω is a $6\times6\times6\times6$ construct where each element Ω_{IJKL} holds weighted averages of orientations g. Equation (9) can be written as

$$\bar{A}_{IJ} = \bar{\Omega}_{IJKL}A_{KL}, \quad I, J, K, L = 1\ldots6. \quad (11)$$

2.1.2. Orientation distribution function. Calculations for both aggregate constants and DECs require the availability of the weight $f(g)$ of the grain orientation g. $f(g)$ is to be understood as a multiple on random density, with 1 denoting complete randomness. For numerical purposes it is assumed that the orientation distribution function (ODF) is available as a tabulation of equidistant {φ_1, Φ, φ_2, weight} values on a $5^\circ\times5^\circ\times5^\circ$ grid. Tabulated output in this format can be produced by most texture analysis codes (Kallend *et al.*, 1991; Hielscher & Schaeben, 2008; Bunge, 1982) and it is the most universal form of ODF representation. The retrieval of the ODF value $f(g) = f(\varphi_1, \Phi, \varphi_2)$ for $g(\varphi_1, \Phi, \varphi_2)$ can be reduced to a look-up of values $f(g)$ in this grid, which is also the fastest way in numerical terms. The ODF must be given sorted (first for φ_1, followed by Φ and then by φ_2) and in fully expanded form, *i.e.* $\varphi_1 = 0\ldots360^\circ$, $\Phi = 0\ldots180^\circ$, $\varphi_2 = 0\ldots360^\circ$, and it is organized in such a way that the ODF value for each of the eight cell vertices (Fig. 3) can be retrieved through simple calculations of the table index. For example, the table index l of the first vertex on the lower-left corner of the cell in Fig. 3 is given by

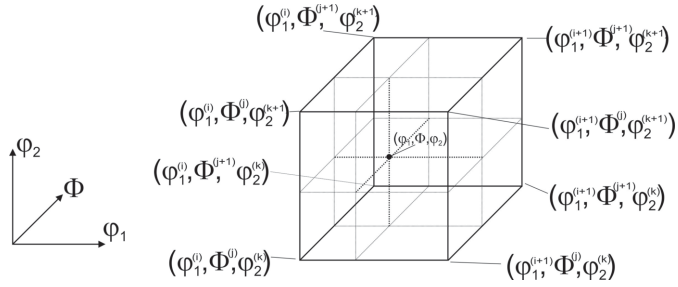

Figure 3
Location of a triplet (φ_1, Φ, φ_2) in Euler space, with ODF values given at each vertex. The indices (i, j, k) are the tabular indices of $f(\varphi_1^{(i)}, \Phi^{(j)}, \varphi_2^{(k)})$. Numbers in parentheses denote the number of the equation used for interpolation at the given location.

$$l = i + j + k$$
$$i = \mathrm{int}(\varphi_1/5)\times37\times73;\ j = \mathrm{int}(\Phi/5)\times73;\ k = \mathrm{int}(\varphi_2/5). \quad (12)$$

The function int() refers to the integer part. The other seven indices can be obtained by adding 1 for the respective direction. The result of the single-index look-up table is a very fast return in computational terms.

The ODF value $f(\varphi_1, \Phi, \varphi_2)$ can be obtained from the following interpolations from the values at the vertices:

$$f_{\varphi_2}^{(1)} = f\left(\varphi_1^{(i)}, \Phi^{(j)}, \varphi_2^{(k)}\right) + \frac{f\left(\varphi_1^{(i)}, \Phi^{(j)}, \varphi_2^{(k+1)}\right) - f\left(\varphi_1^{(i)}, \Phi^{(j)}, \varphi_2^{(k)}\right)}{\varphi_2 - \varphi_2^{(k)}}, \quad (13)$$

$$f_{\varphi_2}^{(2)} = f\left(\varphi_1^{(i)}, \Phi^{(j+1)}, \varphi_2^{(k)}\right) + \frac{f\left(\varphi_1^{(i)}, \Phi^{(j+1)}, \varphi_2^{(k+1)}\right) - f\left(\varphi_1^{(i)}, \Phi^{(j+1)}, \varphi_2^{(k)}\right)}{\varphi_2 - \varphi_2^{(k)}}, \quad (14)$$

$$f_{\Phi}^{(1)} = f_{\varphi_2}^{(1)} + \frac{f_{\varphi_2}^{(2)} - f_{\varphi_2}^{(1)}}{\Phi - \Phi^{(j)}}, \quad (15)$$

$$f_{\varphi_2}^{(3)} = f\left(\varphi_1^{(i+1)}, \Phi^{(j)}, \varphi_2^{(k)}\right) + \frac{f\left(\varphi_1^{(i+1)}, \Phi^{(j)}, \varphi_2^{(k+1)}\right) - f\left(\varphi_1^{(i+1)}, \Phi^{(j)}, \varphi_2^{(k)}\right)}{\varphi_2 - \varphi_2^{(k)}}, \quad (16)$$

$$f_{\varphi_2}^{(4)} = f\left(\varphi_1^{(i+1)}, \Phi^{(j+1)}, \varphi_2^{(k)}\right) + \frac{f\left(\varphi_1^{(i+1)}, \Phi^{(j+1)}, \varphi_2^{(k+1)}\right) - f\left(\varphi_1^{(i)}, \Phi^{(j+1)}, \varphi_2^{(k)}\right)}{\varphi_2 - \varphi_2^{(k)}}, \quad (17)$$

$$f_{\Phi}^{(2)} = f_{\varphi_2}^{(3)} + \frac{f_{\varphi_2}^{(4)} - f_{\varphi_2}^{(3)}}{\Phi - \Phi^{(j)}}, \quad (18)$$

$$f(\varphi_1, \Phi, \varphi_2) = f_{\Phi}^{(1)} + \frac{f_{\Phi}^{(2)} - f_{\Phi}^{(1)}}{\varphi_1 - \varphi_1^{(i)}}. \quad (19)$$

2.2. Overall elastic constants

The overall elastic constants, also referred to as bulk or aggregate elastic constants depending on which micromechanical model is selected, in *IsoDEC* are calculated either through minimization (self-consistent models) or through orientation averaging (arithmetic or geometric).

2.2.1. Models by Voigt, Reuss and Hill. The upper and lower bound models by Voigt and Reuss are based on numerical integration over ODF-weighted grain orientations. What constitutes upper or lower bounds is often illustrated through Young's modulus which is a unidirectional quantity. For example, for isotropic bulk values of Young's modulus E one has $E^{\mathrm{V}} > E^{\mathrm{R}}$.

The calculation of the tensors is performed most efficiently through equation (11) for each phase:

$$\bar{S}_{IJ}^{\mathrm{R}} = \sum_i^M \alpha_i \bar{\Omega}_{IJKL}^{(i)} S_{KL}^{(i)}, \;\; I,J,K,L = 1\ldots6; \;\; i = 1\ldots M; \quad (20)$$

$$\bar{C}_{IJ}^{\mathrm{V}} = \sum_i^M \alpha_i \bar{\Omega}_{IJKL}^{(i)} C_{KL}^{(i)}, \;\; I,J,K,L = 1\ldots6; \;\; i = 1\ldots M. \quad (21)$$

Here, (i) is the index for phase (i), α_i is the given volume fraction for that phase, $\bar{\Omega}_{IJKL}^{(i)}$ contains the orientation average for phase (i), M is the number of phases, and $S_{KL}^{(i)}$ and $C_{KL}^{(i)}$ are the T-transformed single-crystal compliance and stiffness tensors for phase (i).

There are two numerically slightly different arithmetic Hill averages:

$$\bar{S}_{IJ}^{\mathrm{H},1} = \frac{1}{2}\left[\bar{S}_{IJ}^{\mathrm{R}} + \left(\bar{C}^{\mathrm{V}}\right)_{IJ}^{-1}\right], \;\; I,J,K,L = 1\ldots6; \quad (22)$$

$$\left(\bar{C}^{\mathrm{H},2}\right)_{IJ}^{-1} = \frac{1}{2}\left\{\left[\bar{C}^{\mathrm{V}} + \left(\bar{S}^{\mathrm{R}}\right)^{-1}\right]\right\}_{IJ}^{-1}, \;\; I,J,K,L = 1\ldots6. \quad (23)$$

Note that, similarly to the arithmetic Hill averages, two geometric averages can be formed by multiplying (20) with the inverse of (21) and vice versa, after which the matrix square root is taken.

2.2.2. Kröner-type models. Kröner (1958) derived two expressions for the elastic polarization and the elastic susceptibility that are used to obtain the upper and lower bound estimates of the overall elastic constants. Kröner's fourth-rank tensor notation is replaced by T-transformed 6×6 matrices; orientation-dependent quantities are shown as such.

Susceptibility T:

$$T_{IJ}(g) = U_{IK}(g) S_{KJ}^{\mathrm{bulk}}. \quad (24)$$

Polarization R:

$$R_{IJ}(g) = C_{IJ}(g) - C_{IJ}^{\mathrm{bulk}} + C_{IK}(g) U_{KJ}(g). \quad (25)$$

$$\begin{aligned} U_{IJ}(g) &= -V_{IK}^{-1}(g)\left[C_{KJ}(g) - C_{KJ}^{\mathrm{bulk}}\right], \\ V_{IJ}(g) &= C_{IJ}(g) - C_{IJ}^{\mathrm{bulk}} + C_{KJ}^{\mathrm{bulk}} W_{KJ}, \end{aligned} \quad (26)$$

where the tensors U and V are placeholders. The inverse Eshelby tensor W_{IJ} is obtained from the assumption that the grain shape is that of an ellipsoid whose principal axes are aligned with the principal axes of the sample. In the general anisotropic case with a non-spherical grain shape, W_{IJ} is calculated by means of numerical integration, with the most efficient methods discussed by Gavazzi & Lagoudas (1990). In the hypothetical case of non-aligned reference frames, and for anisotropic materials where the grain ellipsoid axes have some common direction not parallel to the sample axis system, the bulk tensor C_{IJ}^{bulk} must be rotated into the ellipsoid axis system using (7). Kröner-type overall elastic constants are determined in iterative schemes where the bulk tensors for compliance and stiffness are refined with a gradient method until the average elastic polarization and elastic susceptibility vanish (Kröner, 1958). The first equation, often referred to as the Kröner model, states that the average elastic polarization must vanish; it is solved for each component of the bulk compliances S_{IJ}^{bulk}:

$$\int T_{IJ}(g) f(g)\, \mathrm{d}g \rightarrow 0. \quad (27)$$

The second equation (inverse Kröner model) describes the elastic susceptibility, and it is solved for the bulk stiffnesses C_{KJ}^{bulk}:

$$\int R_{IJ}(g) f(g)\, \mathrm{d}g \rightarrow 0. \quad (28)$$

The conditions (27) and (28) apply to each component (IJ). The two solutions are identical if there is no texture and the grains are spherical. For triclinic sample symmetry all 21 independent components of the expressions under the integral sign must approach zero for the correct solution of either C^{bulk} or S^{bulk}. The more common case of isotropic symmetry requires the iteration only over two independent components. Kröner gave his solutions for a single-phase material, which, as shown in the following, can be generalized without difficulty to multiphase aggregates:

$$\int\left[\sum_{\mu=1}^{M}\alpha_\mu T_{IJ}^{\mu}(g)f^{(\mu)}(g)\right]\mathrm{d}g\rightarrow 0, \tag{29}$$

$$\int\left[\sum_{\mu=1}^{M}\alpha_\mu R_{IJ}^{\mu}(g)f^{(\mu)}(g)\right]\mathrm{d}g\rightarrow 0. \tag{30}$$

The sums are extended over all M constituents with individual phase fractions α_μ and individual ODFs $f^{(\mu)}(g)$. Note that the inverse Eshelby tensor W_{IJ} must be calculated for each grain shape. If all phases have the same grain shape, then W_{IJ} is the same for all phases. The two solutions are identical if there is no texture and the grains are spherical (Kneer, 1965).

In the case where both texture and non-spherical grains are considered the solutions to (27) and (28) can diverge significantly. It therefore makes sense to form the arithmetic average of both in the same way as the widely used Hill average,

$$C^{\mathrm{bulk}}=\frac{1}{2}[C(r\rightarrow 0)+S^{-1}(t\rightarrow 0)]. \tag{31}$$

2.2.3. Geometric average. The geometric average model was developed specifically to address the questions surrounding the different solutions from upper bound and lower bound models in both Reuss/Voigt and the Kröner-type models. The resulting expression provides a single solution that satisfies the inversion relation

$$\left(\bar{C}^{\mathrm{geo}}\right)^{-1}=\bar{S}^{\mathrm{geo}}. \tag{32}$$

Detailed explanations are given by Matthies *et al.* (2001), so only the fundamentals will be outlined here. The general expression for the geometric average of a square matrix A is

$$\bar{A}^{\mathrm{geo}}=\prod_{i=1}^{N}(A_i)^{w_i}=\left[\prod_{i=1}^{N}(1/A_i)^{w_i}\right]^{-1},\ w_i=\frac{f(g_i)\Delta g_i}{\sum_{j=1}^{N}f(g_j)\Delta g_j}. \tag{33}$$

The w_i ($\sum_{i=1}^{N}w_i=1$) are understood as weights or probabilities of expression of a grain orientation g_i; $f(g_i)$ is the average ODF value in the orientation interval Δg_i. Using the properties of the exponential and logarithm, one obtains

$$\begin{aligned}\bar{A}^{\mathrm{geo}}&=\exp\left(\ln\left\{\prod_{i=1}^{N}[A(g_i)]^{w_i}\right\}\right)\\&=\exp\left(\sum_{i=1}^{N}\ln\left\{W(g_i)A^{(0)}\left[W(g_i)\right]^{-1}\right\}w_i\right),\quad\sum_{i=1}^{N}w_i=1.\end{aligned} \tag{34}$$

The w_i are given explicitly in (33). Using (10) and (11) together with the logarithm property, the matrix exponential (34) becomes

$$\bar{A}^{\mathrm{geo}}=\exp\left[\bar{\Omega}\ln\left(A^{(0)}\right)\right], \tag{35}$$

$$\begin{aligned}\ln\left(A^{(0)}\right)&=V[\ln(A')]V^{-1},\\A'&=V^{-1}A^{(0)}V.\end{aligned} \tag{36}$$

The matrix logarithm $\ln(A^{(0)})$ can be determined through Jacobi diagonalization of $A^{(0)}$ which yields the matrix of eigenvectors V. The natural logarithm is applied only to the diagonal elements of A'. Operations such as the matrix exponential and the matrix square root are calculated by applying the exponential or square root to the diagonal elements of A' instead of the logarithm.

The geometric average for overall elastic constants expressed as the complete orientation average is

$$\bar{S}^{\mathrm{geo}}=\exp\left[\bar{\Omega}\ln\left(S^{(0)}\right)\right]=\left\{\exp\left[\bar{\Omega}\ln\left(C^{(0)}\right)\right]\right\}^{-1}. \tag{37}$$

As mentioned before, the inversion equality (32) holds, thus yielding a unified solution. Nonetheless, the usefulness of (22), (23), (31) and (37) is more rooted in mathematical reasons than in their physical justification. Lastly, the generalization of the geometric average to multiphase aggregates is straightforward:

$$\bar{S}^{\mathrm{geo}}=\exp\left[\sum_{i=1}^{N}\alpha_i\bar{\Omega}_i\ln\left(S_i^{(0)}\right)\right]. \tag{38}$$

N is the number of constituent phases, α_i is the phase fraction and $\bar{\Omega}_i$ is the weighted orientation average for phase i.

2.3. Orientation-correlated grains and DECs

2.3.1. Fundamentals. The orientation selectivity of diffraction allows the measurement of elastic properties of grains with a common lattice vector along a specific sample direction. Elastic constants defined through this property are known as DECs. The fraction of grains involved is generally very small which, together with preferred orientation, may amplify their sensitivity to grain shape, crystal direction (lattice vector) and specimen direction. For a given lattice plane/reflection (*hkl*) and a fixed orientation ($\varphi\psi$) of the lattice vector (also known as the scattering vector) in the specimen coordinate system [$\mathbf{m}\parallel\mathbf{h}\parallel K^{(3)}$, see Fig. 2], a DEC is defined for a specific lattice

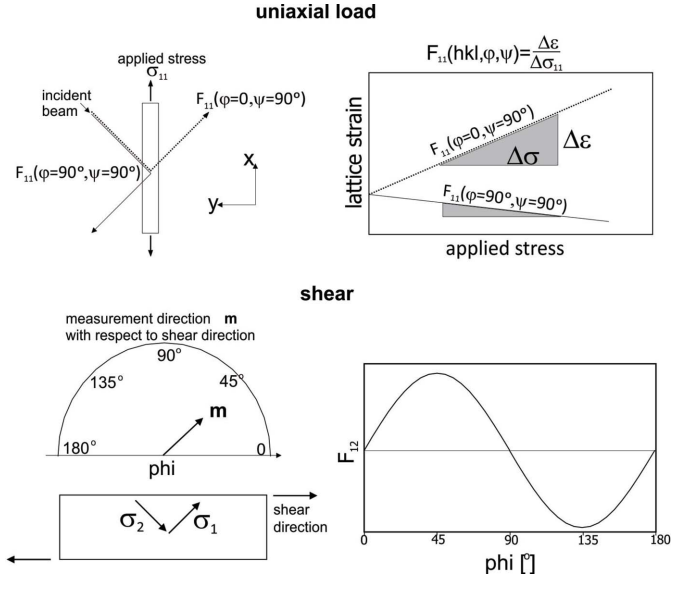

Figure 4
Top: diffraction measurements perpendicular and parallel to the applied stress. Bottom: DEC measurement in shear and the variation of the shear DEC depending on the orientation of the measurement direction **m** with respect to the shear direction SD (φ = 0 → SD ∥ **m**).

plane (*hkl*) and a given specimen direction ($\varphi\psi$) as the slope $\Delta\epsilon/\Delta\sigma$ of lattice strain versus applied stress (Fig. 4). (*hkl*) are the Miller indices of the lattice plane. For measurement purposes, the applied stress should be uniaxial because only in that case is the slope attributable to a single stress component. Existing residual stresses do not change the slope; only the intercept with the strain axis is affected.

One exception to the requirement of applied uniaxial stress is the DEC measurement in pure shear (F_{12}, F_{13}, F_{23}) since a shear stress can be decomposed as the superposition of two mutually perpendicular stress components, one compressive and one tensile, with equal magnitude.

The principal use of DECs is in diffractive stress analysis; however, the dependencies on elastic properties of both the overall aggregate and the properties of the constituent crystallites allow insights into elastic interactions not possible for the aggregate as a whole.

The relationship between lattice strain and applied stress can be expressed through a tensor where the direction **m** of measured strain corresponds to the z direction of the measurement frame K (Fig. 2, centre):

$$\epsilon(hkl, \varphi, \psi) = \epsilon_{33} = \overline{a_{33kl}}(hkl, \varphi, \psi)\bar{\sigma}_{kl}. \tag{39}$$

Note that here and in the following the summation over like indices applies. $\overline{a_{33kl}}(hkl, \varphi, \psi)$ are model-dependent placeholders for components of the orientation-dependent generalized stiffness tensor and $\bar{\sigma}_{kl}$ are the applied stresses. Also, $\overline{a_{33kl}} = \overline{a_{33lk}}$ applies. In the general case of triclinic sample symmetry for a given combination of (*hkl*) and sample direction ($\varphi\psi$), there are six independent DECs. For isotropic sample symmetry that reduces to two independent constants $\overline{a_{33kl}}$ which only depend on (*hkl*).

In the following, the fourth-rank tensor notation is maintained for greater clarity. In the literature (Dölle, 1979; Behnken & Hauck, 1986; Hauk, 1999; Gnäupel-Herold *et al.*, 2012) a collapsed notation is often used which drops the '33' indices:

$$\begin{aligned}\epsilon(hkl, \varphi, \psi) &= F_{11}\bar{\sigma}_{11} + F_{22}\bar{\sigma}_{22} + F_{33}\bar{\sigma}_{33} + 2F_{12}\bar{\sigma}_{12} + 2F_{13}\bar{\sigma}_{13} \\ &\quad + 2F_{23}\bar{\sigma}_{23} \\ F_{kl} &= \overline{a_{33kl}}(hkl, \varphi, \psi).\end{aligned} \tag{40}$$

$F_{kl}(hkl, \varphi, \psi)$ are the DECs or stress factors. The subscripts in F_{kl} denote the specimen direction; mixed '*kl*' denote shears.

An alternative expression is based on the classic equation for diffractive stress analysis on macroscopically isotropic materials (Hauk, 1997):

$$\begin{aligned}&\epsilon(hkl, \varphi, \psi) = \\ &\tfrac{1}{2}s_2(hkl)\left[(\bar{\sigma}_{11}\cos^2\varphi + \bar{\sigma}_{22}\sin^2\varphi + \bar{\sigma}_{12}\sin 2\varphi)\sin^2\psi\right. \\ &\quad \left. + (\bar{\sigma}_{13}\cos\varphi + \bar{\sigma}_{23}\sin\varphi)\sin 2\psi + \bar{\sigma}_{33}\cos^2\psi\right] \\ &\quad + s_1(hkl)(\bar{\sigma}_{11} + \bar{\sigma}_{22} + \bar{\sigma}_{33}).\end{aligned} \tag{41}$$

The values $\frac{1}{2}s_2$ and s_1 depend only on (*hkl*). The relationship between F_{ij} from equation (40) and $\frac{1}{2}s_2$ and s_1 is obtained from parsing (41):

Table 1
DEC notation with respect to directions of applied stress and directions of measurements.

Direction of applied stress	Measurement direction (φ,ψ)	Stress factor notation	Isotropic symmetry
X, ($\varphi = 0$, $\psi = 90$)	($\varphi = 0$, $\psi = 0$)	$F_{11}(0, 0, hkl)$	$-\nu_{hkl}/E_{hkl}$
X, ($\varphi = 0$, $\psi = 90$)	($\varphi = 0$, $\psi = 90$)	$F_{11}(0, 90, hkl)$	$1/E_{hkl}$
X, ($\varphi = 0$, $\psi = 90$)	($\varphi = 90$, $\psi = 90$)	$F_{11}(90, 90, hkl)$	$-\nu_{hkl}/E_{hkl}$
Y, ($\varphi = 90$, $\psi = 90$)	($\varphi = 90$, $\psi = 90$)	$F_{22}(90, 90, hkl)$	$1/E_{hkl}$
Z, ($\varphi = 0$, $\psi = 0$)	($\varphi = 0$, $\psi = 0$)	$F_{33}(0, 0, hkl)$	$1/E_{hkl}$
XY, ($\varphi = 0$, $\psi = 90$)	($\varphi = 45$, $\psi = 90$)	$F_{12}(45, 90, hkl)$	$(1 + \nu_{hkl})/2E_{hkl}$†
XZ, ($\varphi = 0$, $\psi = 0$)	($\varphi = 0$, $\psi = 45$)	$F_{13}(90, 45, hkl)$	$(1 + \nu_{hkl})/2E_{hkl}$†
YZ, ($\varphi = 90$, $\psi = 90$)	($\varphi = 90$, $\psi = 45$)	$F_{23}(90, 45, hkl)$	$(1 + \nu_{hkl})/2E_{hkl}$†

† For shear components the applied stress direction is the shear direction.

$$F_{ij} = \begin{pmatrix} s_1 + \frac{1}{2}s_2\cos^2\varphi\sin^2\psi & 0.5\frac{1}{2}s_2\sin 2\varphi\sin^2\psi & 0.5\frac{1}{2}s_2\cos\varphi\sin 2\psi \\ 0.5\frac{1}{2}s_2\sin 2\varphi\sin^2\psi & s_1 + \frac{1}{2}s_2\sin^2\varphi\sin^2\psi & 0.5\frac{1}{2}s_2\sin\varphi\sin 2\psi \\ 0.5\frac{1}{2}s_2\cos\varphi\sin 2\psi & 0.5\frac{1}{2}s_2\sin\varphi\sin 2\psi & s_1 + \frac{1}{2}s_2\cos^2\psi \end{pmatrix}. \tag{42}$$

Equation (41) cannot be used for anisotropic materials.

The overbar $\overline{a_{33kl}}$ in (39) signifies the average over grain orientations/rotations about the lattice plane normal $\mathbf{h} \parallel \mathbf{m}$. The average is calculated from

$$\begin{aligned}F_{kl}(hkl, \varphi, \psi) = \overline{a_{33kl}} &= \frac{m_i m_j \int_0^{2\pi} a_{ijkl}(g) f(g)\,\mathrm{d}\lambda}{\int_0^{2\pi} f(g)\,\mathrm{d}\lambda}, \\ i, j, k, l &= 1 \ldots 3.\end{aligned} \tag{43}$$

Note that the triple '*hkl*' always denotes Miller indices; the use of k and l in subscripts is unrelated. $f(g)$ was introduced earlier as the weight factor (multiple of random density) or intensity of the ODF for the orientation $g(\varphi_1, \Phi, \varphi_2)$. The angle λ is the rotation angle about the plane normal $\mathbf{h} \parallel \mathbf{m}$ (Fig. 2, left). The measurement direction **m** in the sample coordinate system is

$$\mathbf{m} = \begin{pmatrix} \cos\varphi\sin\psi \\ \sin\varphi\sin\psi \\ \cos\psi \end{pmatrix}. \tag{44}$$

The angles φ and ψ are defined in Fig. 2. The subscript indices k and l relate to the sample directions in Fig. 4 in the way demonstrated in Table 1.

The DEC models discussed in the following were selected or developed because they are conceptually suitable for including the effects of preferred orientation. The inclusion of texture through the ODF is a problem of numeric programming; therefore, all DEC models discussed here include the ODF in the same manner through the weights $f(g)$ obtained as described earlier.

First, a functional relationship between the direction **m** in the sample coordinate system and the lattice plane normal **h** in

the crystal coordinate system is needed to perform the integration in (43). While some crystal symmetries allow equation (43) as a closed expression (Möller & Martin, 1939; Gnäupel-Herold *et al.*, 1998; Behnken & Hauck, 1986), the thus-derived equations are very complex and offer no benefit either numerically or for general understanding. The relationship (43) is derived by considering the coordinate system of the sample K_A, the orthonormal crystal system K_B and the intermediate measurement system K. Its z direction $K^{(3)}$ is parallel to the measurement direction **m** and the crystal direction **h** linked through the rotations g_1 and g_2.

In Bunge notation (Bunge, 1982) the orientation of the intermediate system K is expressed through the rotation matrix $g(\varphi_1, \Phi, \varphi_2)$. Specifically, g in equation (3) is the rotation $K_B \rightarrow K_A$ for grains where the lattice vector **h** is parallel to the measurement direction **m**. Using the intermediate coordinate system, K can be expressed as the product of two rotations, g_1 ($K_A \rightarrow K$) and g_2 ($K_B \rightarrow K$) (Bunge, 1982):

$$g(\varphi_1, \Phi, \varphi_2) = g_2\left(\lambda, \Phi_B, \tfrac{\pi}{2} - \beta_B\right) g_1\left(\varphi + \tfrac{\pi}{2}, \psi, 0\right), \tag{45}$$

$$g_1\left(\varphi + \tfrac{\pi}{2}, \psi, 0\right) = \begin{bmatrix} \cos\left(\varphi + \frac{\pi}{2}\right) & \sin\left(\varphi + \frac{\pi}{2}\right) & 0 \\ -\sin\left(\varphi + \frac{\pi}{2}\right)\cos\psi & \cos\left(\varphi + \frac{\pi}{2}\right)\cos\psi & \sin\psi \\ \sin\left(\varphi + \frac{\pi}{2}\right)\sin\psi & -\cos\left(\varphi + \frac{\pi}{2}\right)\sin\psi & \cos\psi \end{bmatrix}, \tag{46}$$

$$g_2\left(\lambda, \Phi_B, \tfrac{\pi}{2} - \beta_B\right) = \ldots = \begin{pmatrix} \cos\lambda\cos B_B & \sin\lambda\cos B_B & \sin B_B \sin\Phi_B \\ -\sin\lambda\sin B_B\cos\Phi_B & +\cos\lambda\sin B_B\cos\Phi_B & \\ -\cos\lambda\sin B_B & -\sin\lambda\sin B_B & \cos B_B\sin\Phi_B \\ -\sin\lambda\cos B_B\cos\Phi_B & +\cos\lambda\cos B_B\cos\Phi_B & \\ \sin\lambda\sin\Phi_B & -\cos\lambda\sin\Phi_B & \cos\Phi_B \end{pmatrix}. \tag{47}$$

Here, $B_B = \frac{\pi}{2} - \beta_B$. The meaning of the angles ψ, φ, λ, Φ_B, β_B is shown in Fig. 2. Note that the use of φ, ψ as spherical polar angles in the sample system S is common throughout the literature; Bunge used γ_A and Φ_A instead ($\gamma_A = \varphi$, $\Phi_A = \psi$). Φ_B and β_B are spherical polar angles in the crystal orthonormal system K that determine the direction of the lattice plane normal **h**. They are calculated with Miller indices (hkl) for the general case of a triclinic crystal system with lattice parameters a, b, c, α, β, γ as

$$\Phi_B = \arccos\left(h_z / \sqrt{h_x^2 + h_y^2 + h_z^2}\right), \tag{48a}$$

$$\beta_B = \arccos\left(h_x / \sqrt{h_x^2 + h_y^2}\right), \tag{48b}$$

$$\mathbf{h} = \begin{pmatrix} h_x \\ h_y \\ h_z \end{pmatrix} = \begin{bmatrix} h/a \\ -h/a\cot\gamma + k/(b\sin\gamma) \\ hbc\sin\alpha\frac{\cos\alpha\cos\gamma - \cos\beta}{V\sin\alpha\sin\gamma} + kac\sin\beta\frac{\cos\beta\cos\gamma - \cos\alpha}{V\sin\beta\sin\gamma} + \frac{lab\sin\gamma}{V} \end{bmatrix}. \tag{49}$$

The volume of the unit cell is

$$V = abc\sqrt{1 + 2\cos\alpha\cos\beta\cos\gamma - \cos^2\alpha - \cos^2\beta - \cos^2\gamma}.$$

Equations (44)–(49) allow the evaluation of the integral in (43) once $a_{ijkl}(g)$ is specified. The weight $f(g)$ is determined from the ODF by first explicitly multiplying (47) and (46), and subsequently using inverse trigonometric functions to obtain values for $\varphi_1, \Phi, \varphi_2$ from the matrix g in (45) or (3). The detailed procedure for obtaining $f(g)$ from values $\varphi_1, \Phi, \varphi_2$ is explained in Section 2.1.2. The equations for obtaining $\varphi_1, \Phi, \varphi_2$ from (3) are

$$\begin{aligned} \varphi_1 &= \tan^{-1}\frac{g_{31}}{g_{32}}, \quad \sin\Phi \neq 0, \\ \varphi_2 &= \tan^{-1}\frac{g_{13}}{g_{23}}, \quad \sin\Phi \neq 0, \\ \Phi &= \cos^{-1} g_{33}. \end{aligned} \tag{50}$$

For the case of $\Phi = 0$, (50) cannot be used; instead φ_1 is calculated from

$$\varphi_1 = \frac{1}{2}\tan^{-1}\frac{g_{12}}{g_{11}}, \quad \varphi_2 = -\varphi_1. \tag{51}$$

Once the triple $\varphi_1, \Phi, \varphi_2$ has been determined, the numerical value $f(\varphi_1, \Phi, \varphi_2)$ can be obtained from the look-up table as described earlier.

The numerical advantages in performing the calculation (43) in the notation of T-transformed [see (4) and (5)] matrices have been discussed earlier; however, mixing the two-index notation of F_{kl} and the components of the vector **m** from (43) on one side with the matrix notation above on the other side is confusing. Hence, the following expressions for DECs will be derived in terms of fourth-rank tensors.

2.3.2. Reuss, Voigt and Hill models. The following equations are the basis for implementations of the most basic DEC models. The Reuss assumption is that of homogeneous stress in all grains (Möller & Martin, 1939), while the Voigt model is the same as for the bulk material (Voigt, 1928) in assuming homogeneous strain. The modified Voigt model (Murray & Noyan, 1999) averages the orientation-dependent stiffnesses, and then takes the inverse of the average. The Hill and geometric Hill models are based on the arithmetic and geometric averages of Reuss and Voigt.

Reuss:

$$a_{ijkl}(g) = s_{ijkl}(g) = g_{im}^{-1} g_{jn}^{-1} g_{ko}^{-1} g_{lp}^{-1} s_{ijkl}. \tag{52}$$

Voigt:

$$a_{ijkl} = \bar{c}^{-1}_{ijkl}. \tag{53}$$

Modified Voigt:

$$a_{ijkl}(g) = \left(g^{-1}_{im} g^{-1}_{jn} g^{-1}_{ko} g^{-1}_{lp} c_{mnop}\right)^{-1}_{ijkl}. \tag{54}$$

Hill:

$$a_{ijkl}(g) = \tfrac{1}{2}\left[s_{ijkl}(g) + \bar{c}^{-1}_{ijkl}\right]. \tag{55}$$

Geometric Hill:

$$a_{ijkl}(g) = \left[s(g)\bar{c}^{-1}\right]^{-1/2}_{ijkl}. \tag{56}$$

c_{ijkl} and s_{ijkl} are the single-crystal stiffnesses and compliances, respectively. The dependence of $a_{ijkl}(g)$ on (hkl) and on the measurement direction is rooted in equations (45)–(51). The Voigt model is independent of (hkl). The square root in (56) implies a matrix square root and it requires the Voigt matrix notation (4); the T transformation (5) is optional because of the previously discussed advantages.

2.3.3. Kröner-type models. The expressions for upper and lower bound single orientation grain compliances were given by Kröner (1958).

Kröner:

$$a_{ijkl}(g) = S_{ijkl} + u_{ijmn}(g) S_{mnkl}. \tag{57}$$

Inverse Kröner:

$$a_{ijkl}(g) = \left[c_{ijkl}(g) + c_{ijmn}(g) u_{mnkl}(g)\right]^{-1}. \tag{58}$$

Average Kröner (DEC):

$$a_{ijkl}(g) = \tfrac{1}{2}\left\{S_{ijkl} + u_{ijmn}(g) S_{mnkl} + \left[c_{ijkl}(g) + c_{ijmn}(g) u_{mnkl}(g)\right]^{-1}\right\}. \tag{59}$$

S_{ijkl} are the compliances of the aggregate (bulk). The expression for the average was not given by Kröner, but its use for the calculation of DECs is straightforward and analogous to the Hill average. Note that (59) cannot be used to calculate overall elastic constants. The two quantities $u_{ijkl}(g)$ and $v_{ijkl}(g)$ are defined as

$$\begin{aligned} u_{ijkl}(g) &= u_{ijkl}(g) = -v^{-1}_{ijmn}(g)\left[c_{mnkl}(g) - C_{mnkl}\right], \\ v_{ijkl}(g) &= c_{ijkl}(g) - C_{ijkl} + C_{ijmn} w_{mnkl}. \end{aligned} \tag{60}$$

$c_{ijkl}(g)$ are orientation-dependent single-crystal stiffnesses and C_{ijkl} are the bulk stiffnesses. The tensor w_{mnkl} is the inverse Eshelby tensor. The methods for the calculation of the Eshelby tensor in the general, anisotropic case were outlined by Eshelby (1957) and Gavazzi & Lagoudas (1990).

2.3.4. Geometric average. The geometric average according to Matthies *et al.* (2001) is a construct based on a goal to achieve the inversion equality (32). Note that matrix exponentials, logarithms and matrix square roots are needed in the following which require matrix notation. Equations (33)–(38) apply, with the orientations $g = g(\lambda)$ taken along the rotation angle λ. $\bar{\Omega}$ in (37) is replaced by the path integral:

$$\bar{\Omega}^{(\lambda)}_{IJKL} = \frac{\int_0^{2\pi} W(g)_{IK} W(g)_{JL} f(g)\,\mathrm{d}\lambda}{\int_0^{2\pi} f(g)\,\mathrm{d}\lambda}, \quad I, J, K, L = 1 \ldots 6. \tag{61}$$

λ is the rotation angle about the scattering vector, and the orientations $g(\varphi_1, \Phi, \varphi_2)$ for a particular λ are calculated using (45)–(49). The $\overline{a_{33kl}}$ from (43) in matrix notation are written as (Matthies *et al.*, 2001)

$$\bar{A}^{(\lambda),\mathrm{geo}} = \exp\left[\overline{\Omega}^{(\lambda)} \ln(S)\right]. \tag{62}$$

The superscript λ indicates the geometric average over the orientations along the rotation angle; S are the single-crystal compliances in matrix form. Equation (62) yields results that generally differ by small percentages from Kröner-type calculations, with (62) being faster computationally. Differences become larger if grain shapes deviate more strongly from spheroid shapes since there is no mechanism for including shape effects. In order to establish a relationship with the bulk stiffness tensor S^{bulk}, and to allow calculations for multiphase aggregates, Matthies *et al.* (2001) postulated the following relationship as the matrix square root:

$$\bar{A}^{(\lambda,\mathrm{bulk}),\mathrm{geo}} = \sqrt{\bar{A}^{(\lambda),\mathrm{geo}} S}. \tag{63}$$

The matrix square root is calculated in the same way as (36) by taking the square root of the diagonal elements instead of the logarithm. The stress factors from equation (43) are obtained by transforming $\bar{A}^{(\lambda,\mathrm{bulk}),\mathrm{geo}}$ back to tensor form.

2.3.5. Other DEC models. Among the DEC models not mentioned here are those of de Wit (1997), van Leeuwen *et al.* (1999) and Baczmanski *et al.* (2006). The first is limited in scope to cubic and hexagonal materials without preferred orientation, while the others make assumptions about the states of strain and stress in the crystallites that are only suitable for thin films or X-ray measurements, thus limiting their generality. Numerous other models can be constructed through different assumptions about grain–matrix interaction or boundary conditions; however, such models do not yield results notably different from what was discussed in previous sections.

2.3.6. DECs from electron backscatter diffraction data. A given electron backscatter diffraction (EBSD) data set contains grain orientations (Euler angles), grain centre-of-gravity coordinates, ellipsoid axis parameters (grain shape approximated as ellipse), ellipsoid tilt angle, grain area and the number of neighbour grains. All models discussed previously can operate on a discrete set of grains. Voigt/Reuss/Hill models can utilize grain orientations and weights whereas Kröner-type models and the geometric average are sensitive to the overall elastic constants as well. Kröner-type models can incorporate additional information through the ellipsoid axis parameters, the orientation of the shape ellipse and the elastic properties of the surrounding grains. Consider a grain oriented for diffraction. The crystallites directly surrounding the diffracting grain constitute the 'local matrix'. In the presence of macroscopic stresses strain fields arise if there are

differences between the elastic constants of the grain and its surroundings. Generally, the strain fields decay to small fractions of their magnitude at the interface within one grain diameter (Mura, 1987; Sato *et al.*, 1979). Therefore, it can be argued that the properties of the local matrix have a dominant effect on the magnitude of the grain–matrix interaction compared with properties of the overall aggregate. In the absence of orientational correlations between neighbouring grains, properties of the local matrix will on average be equal to those of the overall matrix. Differences between a local matrix and the general bulk can arise after processes such as twinning or the formation of martensite inside grains. Other possible reasons for a local matrix effect are bimodal textures where two strong texture components pair two different crystal directions in the same sample direction. Examples are found in sheet metal forming textures of steel (Creuziger *et al.*, 2014) where γ-fibres [(111) ∥ ND] sometimes occur together with cube- and Goss-type textures [(100) ∥ ND], thus leading to grains with orientations (111) ∥ ND preferentially surrounding grains with orientations (100) ∥ ND (Fig. 5).

In order to use any of the aforementioned models, the first step is to identify grains in the EBSD data set that are oriented for diffraction with (*hkl*) as the reflection and **m** ($\varphi\psi$) as the measurement direction. It is understood that the reflection (*hkl*) corresponds to a crystal direction **h** which is obtained from (*hkl*) through (48*a*), (48*b*) and (49) for orthogonal crystal systems or through the general formulas given by Gnäupel-Herold *et al.* (2012). The three Euler angles are calculated from equations (3)–(51), and using n discrete values for the angle λ by dividing the interval $\{0, 2\pi\}$ for λ into n = round$(2\pi/\delta)$ sub-intervals, where δ is the allowable misorientation angle. The meaning of δ can be understood as a mosaic or detector opening within which misaligned grains still contribute to diffraction. For example, a value $\delta = 5^\circ$ leads to $n = 72$ sets of Euler angles $(\varphi_1, \Phi, \varphi_2)_i^{(\lambda)}$ that are compatible with the reflection (*hkl*) in the sample direction ($\varphi\psi$). The procedure is repeated for m permutations of (*hkl*) compatible with the crystal symmetry. For cubic symmetry there are $m = 24$ such permutations, resulting in 24×72 orientations that are compared with all p orientations listed in the EBSD data set. An EBSD grain is oriented for diffraction if the misorientation angle is within δ. The numerical demands are considerable – the number of operations involving numerous matrix multiplications is $m \times n \times p$. The misorientation angle is defined as (Bunge, 1982)

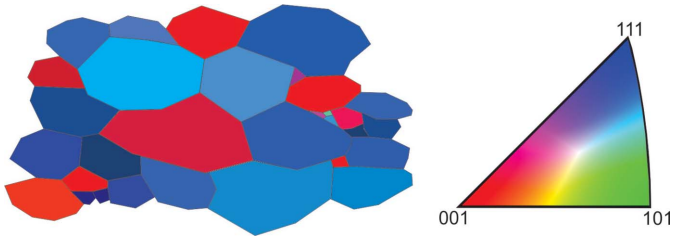

Figure 5
Simulated grain structure in which (111)-oriented grains frequently surround (100)-oriented grains.

$$g(\varphi_1, \Phi, \varphi_2) = g_2\left(\varphi_1^{(\mathrm{EBSD})}, \Phi^{(\mathrm{EBSD})}, \varphi_2^{(\mathrm{EBSD})}\right)_j \times g_1^{-1}\left(\varphi_1^{(\lambda)}, \Phi^{(\lambda)}, \varphi_2^{(\lambda)}\right)_i, \quad (64)$$

$$\delta = \cos^{-1}\left(\frac{g_{11} + g_{22} + g_{33} - 1}{2}\right).$$

The orientation matrices g_1 and g_2 are calculated from (3). g_1^{-1} is the inverse of g_1.

Once a grain oriented for diffraction is identified, the neighbouring grains are found through the distance measure

$$d \leq \sqrt{(x_i - x_j)^2 + (y_i - y_j)^2} \quad i, j = 1 \ldots N. \quad (65)$$

Here, d is sensibly chosen as the grain diameter and N as the number of grains. If no neighbour is found, d should be increased incrementally until the number of neighbours noted in the EBSD data set agrees with or exceeds the number of matches from (65). Once the neighbouring grains are found, the local matrix constants can be calculated through any of the previously discussed methods.

2.4. Fitting of SCECs

As previously shown, DECs retain a damped form of single-crystal elastic behaviour along the lattice vector determined by (*hkl*). Therefore, the functional relationships between DECs and SCECs allow the solution of the inverse problem in which single-crystal constants are obtained from measured DECs. Closed expressions relating SCECs and DECs can be derived for higher crystal symmetries, but SCECs are generally best determined through the least-squares fitting of SCECs using one of the models. Such a refinement is fundamentally no different from fitting a peak function to a diffraction peak. The quantity to minimize is

$$\chi^2 = \sum_{n=1}^{N}\left\{\frac{F_{ij}^{(\mathrm{m},n)}\left[(hkl)_n, \varphi_n, \psi_n\right] - F_{ij}^{(\mathrm{c},n)}\left[(hkl)_n, \varphi_n, \psi_n\right]}{\sigma\left(F_{ij}^{(\mathrm{m},n)}\right)}\right\}^2 \rightarrow \min. \quad (66)$$

The sum can contain any combination of F_{11}, F_{22}, F_{33}, F_{23}, F_{13} and F_{12}. The superscripts 'm' (measured) and 'c' (calculated) indicate the $n = 1 \ldots N$ measured and calculated DECs, the latter using any of the models discussed previously.

3. Results and calculations

3.1. Overall elastic constants

The calculation of overall elastic constants using the models by Hill (Reuss and Voigt are implied) for multiphase materials without texture is commonplace and numerically simple. Some minor difficulty arises in the presence of preferred orientation since now integration in Euler space $(\varphi_1, \Phi, \varphi_2)$ is required. In this work, the Kröner-type models are the most powerful means of estimating overall elastic constants due to their built-in grain–matrix interaction. As mentioned before, both the Kröner model and the inverse represent bounds on the elastic

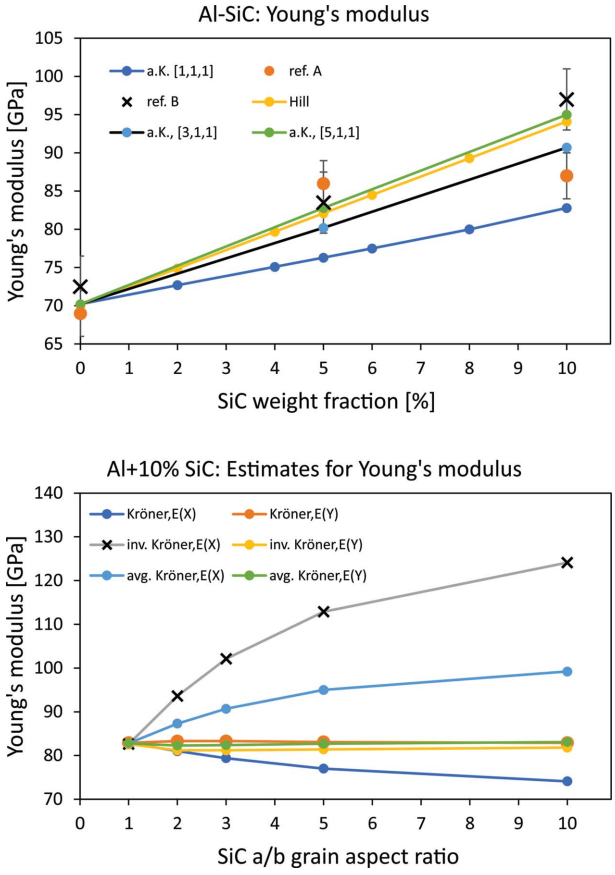

Figure 6
Top: comparison of predicted and measured Young's modulus for an Al–SiC composite using the Hill average, average Kröner and measured values (reference A: Pal *et al.*, 2009; reference B: Suryanarayana, 2011). Bottom: the sensitivity of Kröner-type models with respect to both grain shape and the direction of alignment of the grains. Experimental data were not provided with information on grain shapes. The grain axes (a, b, c) are aligned with sample directions (x, y, z) but are uncorrelated with crystallographic axes.

constants but both exhibit only small differences for spherical grains. An example with calculations for a composite of aluminium and silicon carbide is given here.

Fig. 6 indicates that the Hill average agrees well with the measured values. The average Kröner agrees similarly well if SiC fibres with an ellipsoidal shape [5, 1, 1] aligned along the X direction are assumed (numbers in brackets denote ellipsoid aspect ratios). It is also revealed that the grain shape plays a significant role in Kröner-type models which are the only models sensitive to the grain shape. Overall, for materials with modest anisotropy the Hill averages, the average Kröner model and the geometric average yield very similar values. Larger differences between models are revealed in mixtures of phases with large elastic disparities or materials with large elastic anisotropy.

3.2. DECs from EBSD data

Data from EBSD contain orientations, shape parameters and coordinates of individual grains, thus allowing the extraction of information that can be used in Kröner-type models. In order to investigate the effects of individual grain neighbourhoods on the DECs, two equal-weight data sets were generated using an ODF based on neutron diffraction pole figures from a mild steel deformed to 20% plane strain along the transverse direction. Calculated pole figures are shown in Fig. 7. The granularity of the EBSD pole figure is the result of the limited size of the data set (67 × 67 orientations).

In the first data set grain orientations and coordinates were uncorrelated; the second data set was set up such that (h00)-type grains oriented in the ND [(100) ∥ (φ = 0, ψ = 0)] were surrounded by grains with the orientation [(111) ∥ (φ = 0, ψ = 0)] within a misorientation of 5°. In other words, grains from the central pole of the (200) pole figure were only directly surrounded by grains of the central pole of the (222) pole figure. Note that ODFs and pole figures generated from the correlated and uncorrelated data sets are identical. Grains were arranged on a 67 × 67 grid. The misorientation-angle distribution for both data sets is shown in Fig. 8.

The large spike at 0° is the result of (111) neighbours with the same orientation due to the data set being organized with all grains having the same size. On the level of small sub-populations of grains oriented along ND = (φ = 0, ψ = 0) the grain-to-neighbour misorientation shows appreciable differences between correlated and uncorrelated orientations only for (200)- and (222)-oriented grains. In the correlated data set the average grain–neighbour misorientation for (200) is 49.3° which is within 5° of the ideal angle ∠([100][111]) with the plane normal. Grains with (222) orientation in the correlated data set show lower average grain–neighbour misorientation

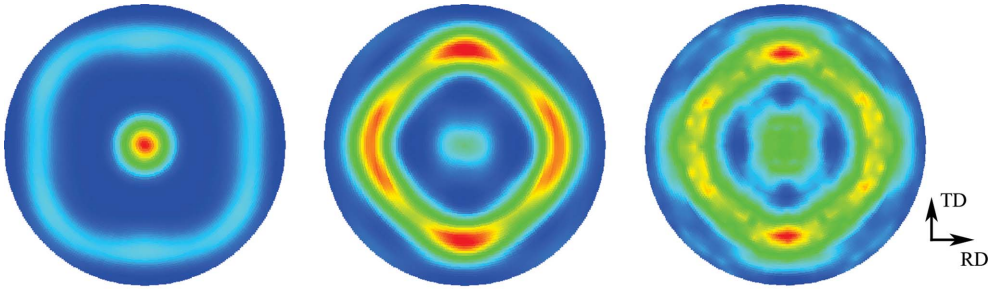

Figure 7
Neutron diffraction pole figures for (222) and (200) reflections for a mild steel deformed to 20% plane strain along the transverse direction (TD). The pole figures '(200), EBSD' for correlated and uncorrelated data sets are identical. RD, rolling direction.

because a large number of them are direct neighbours of other (222) grains.

The calculation of DECs $F_{11}(0, 0)$ $(= -\nu/E)$ shows that the largest effect of correlated orientations is found for $F_{11}(200, 0, 0)$ (see Fig. 9, the difference between symbols at $\Gamma = 0$). A smaller shift (compared with uncorrelated grains) is found for $F_{11}(222, 0, 0)$ (Fig. 9 at $\Gamma = 1/3$), but both reflections show the expected shift to directionally greater elastic stiffness on account of preferential pairings with elastically hard (111)-oriented grains.

Overall, all values $F_{11}(hkl, 0, 0)$ slightly increased compared with the ODF-based calculation, which is not the case for $F_{11}(hkl, 0, 90°)$ $(= 1/E)$ (Fig. 9). The latter is specific for the rolling direction (RD), and it is therefore not affected by the (100)-to-(111) orientation correlation in the ND direction. Moreover, the grain-based values are nearly identical to the ODF-based values. This suggests that even without correlated orientations there can be systematic shifts in DEC values for those sample directions that coincide with strong preferred grain orientations. Only such preferred orientations (= large number of grains in this orientation) of the type (111) or (100) will show this effect because the magnitude of the effect depends on the difference with respect to the average orientation. Elastic properties of high-multiplicity reflections are very close to the isotropic average, meaning that grains surrounded only by, for example, (211) ‖ ND grains will not behave very differently from those surrounded by random orientations.

3.2.1. The role of texture. Preferred orientation affects DECs to a much larger extent than bulk elastic properties. The path integral in (43) averages over a fibre in Euler space, and it can have an outsized influence in some combinations of sample direction and reflection (*hkl*) even for weak textures. One of the most prominent examples of highly nonlinear directional effects of texture is the (211) reflection for ferritic steels between the ND and in-plane directions (RD and TD – transverse direction) (Barral *et al.*, 1987; Brakman, 1983;

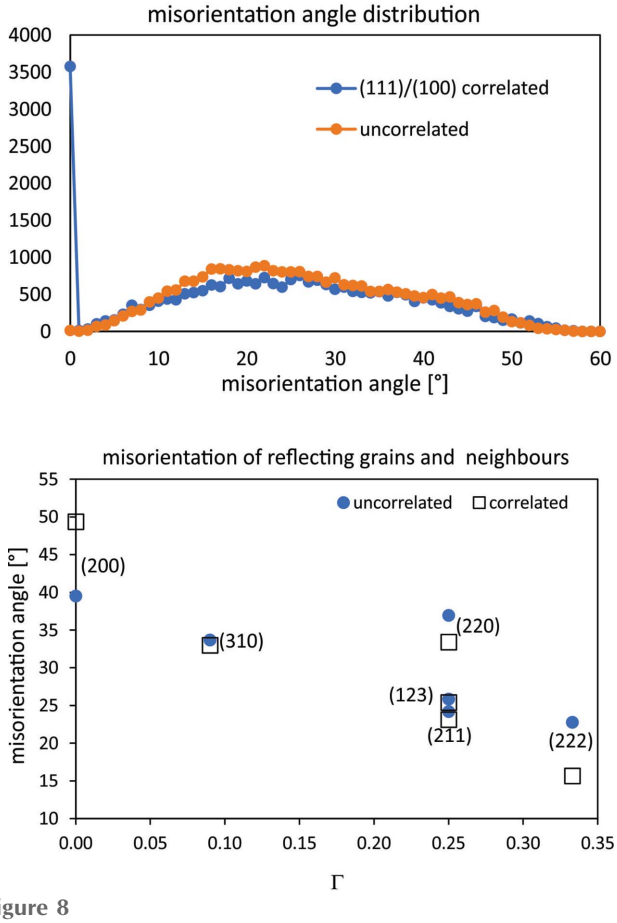

Figure 8
Top: misorientation-angle distributions for an uncorrelated data set and a data set where [(111) ‖ ($\varphi = 0$, $\psi = 0$)] grains were paired with [(100) ‖ ($\varphi = 0$, $\psi = 0$)]-oriented grains. Bottom: average misorientation between grains reflecting in ND = ($\varphi = 0$, $\psi = 0$) and their direct neighbours. The orientation parameter on the x axis is defined as $\Gamma = (h^2k^2 + h^2l^2 + k^2l^2)/(h^2 + k^2 + l^2)^2$. $\Gamma = 0$ corresponds to (h00)-type reflections while $\Gamma = 1/3$ corresponds to (hhh)-type reflections.

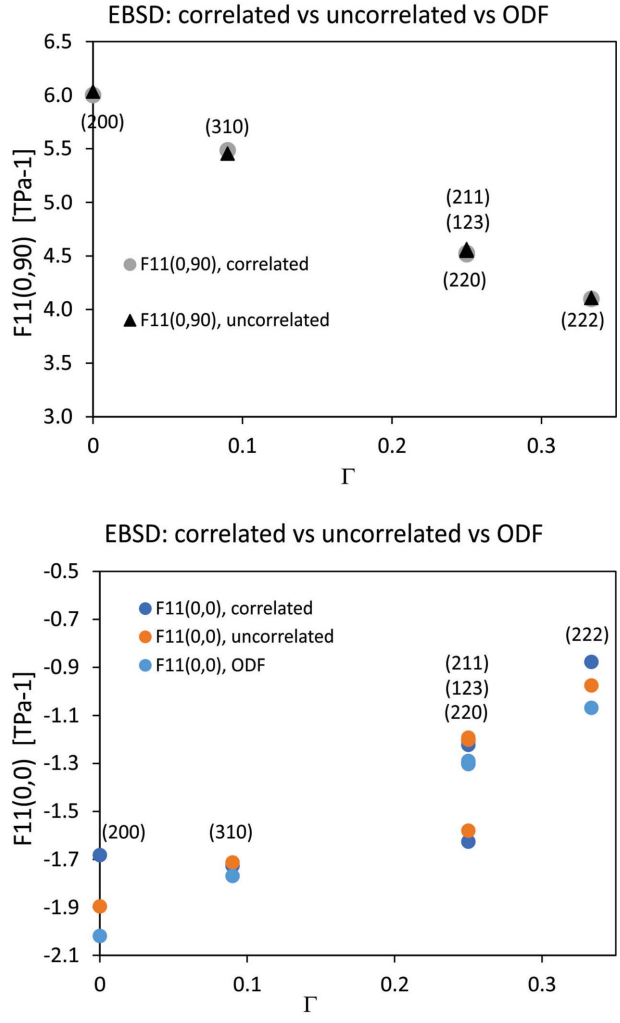

Figure 9
DECs $F_{11}(hkl, 0, 90°)$ $(= 1/E_{hkl})$ (top) and $F_{11}(hkl, 0, 0)$ $(= -\nu_{hkl}/E_{hkl})$ (bottom) for different reflections using correlated grains, uncorrelated grains and the ODF (that was used to generate the EBSD data sets) for quasi-continuum calculations. The ODF-based values for $F_{11}(hkl, 0, 90°)$ are not shown but are nearly identical to the grain-based values. All calculations used the average Kröner model.

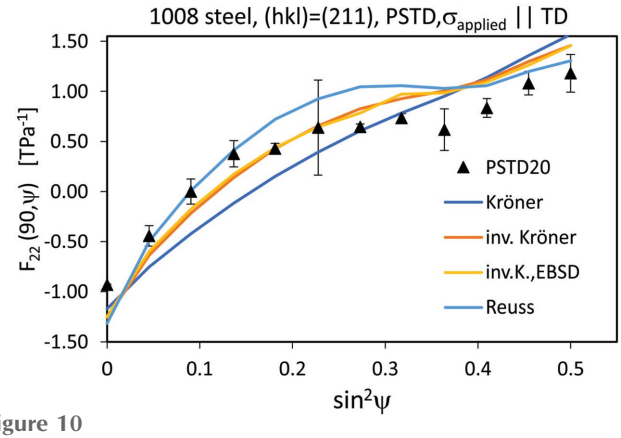

Figure 10
Comparison of measured DECs $F_{22}(211, 90°, \psi)$ with model calculations. The tilt plane in this measurement was between ND ($\varphi = 90$, $\psi = 0$) and TD ($\varphi = 90$, $\psi = 90$). The measurements were performed on a tensile specimen extracted from the 20% plane strain sample deformed in the TD direction.

Gnäupel-Herold *et al.*, 2012). A model's ability to match the observed shape of the directional dependence of the DECs determines directly the accuracy of stress determination for measurements performed in the same directions. In the same way, model accuracy affects the fitting of SCECs. The comparison in Fig. 10 shows the accuracy improvements made through the development of the inverse Kröner model compared with the widely used Reuss and Kröner models. The material discussed in Section 3.2 was used. Nonetheless, applied stress evaluation experiments on a similarly textured material (Gnäupel-Herold *et al.*, 2011) have shown that improvements are still needed. Note that the stress factor $F_{22}(211,90°,\psi)$ indicates an applied stress in the TD direction and a ψ-tilt plane parallel to the ND–TD plane.

3.3. Fitting of SCECs

Fitting of SCECs using DEC data has recently received increased attention for characterizing the elastic constants of alloys where the constituent fractions are sufficiently large that one may expect larger differences from data of pure materials. The preference of specific models in the fitting of SCECs has not yet been analysed in the literature. It is the purpose of the following sections to discuss model suitability and requirements of experimental data with respect to fitting SCECs.

3.3.1. Suitability of the DEC model for fitting SCECs. The most consequential question regarding the use of DEC model fitting relates to aspects of model suitability for obtaining SCECs. In order to analyse the roles of goodness of fit, fit stability and the effect of uncertainties, and to facilitate a broader model comparison, a synthetic data set was created by calculating the DECs using the Kröner-type models, Reuss, Voigt, Hill and the geometric average, and calculating the average over all models. Input single-crystal values for α-titanium were taken from Fisher & Renken (1964). Uncertainties (1σ) were estimated by taking the inverse of the square root of the (*hkl*) multiplicity as a measure of intensity. Each uncertainty was multiplied with a different random number in the range $[-2, 2]$ and added to the respective DEC value, thus disturbing the model value in the range 2σ. Input and fitted DEC values are listed in Table 2.

Overall elastic constants in models with grain–matrix interaction (Kröner-type and geometric average) were updated at every iteration. Remarkably, Reuss, Kröner-type models and Hill (arithmetic average) yield identical DEC results and goodness-of-fit measures but different fitted single-crystal values. The same procedure was also applied to orthorhombic α-uranium, iron and titanium with different

Table 2
Input values and fit results for a simulated data set for titanium.

(*hkl*)	φ (°)	ψ (°)	$F_{11}(\varphi, \psi)$ ($\times$TPa^{-1})	σ ($\times$TPa^{-1})	Reuss, Kröner, inverse Kröner, average Kröner, Hill ($\times$TPa^{-1})	Voigt	Geometric average	Modified Voigt
100	0	0	−2.825	0.218	−2.977	−2.759	−2.972	−2.967
100	0	90	9.492	0.218	9.117	8.721	9.108	9.099
002	0	0	−2.106	0.204	−2.145	−2.759	−2.145	−2.154
002	0	90	7.869	0.204	7.574	8.721	7.575	7.576
101	0	0	−2.881	0.100	−2.868	−2.759	−2.871	−2.873
101	0	90	9.047	0.100	8.926	8.721	8.931	8.938
102	0	0	−2.535	0.213	−2.639	−2.759	−2.638	−2.636
102	0	90	8.615	0.213	8.506	8.721	8.504	8.499
110	0	0	−3.124	0.167	−2.977	−2.759	−2.972	−2.967
110	0	90	9.006	0.167	9.117	8.721	9.108	9.099
103	0	0	−2.523	0.141	−2.463	−2.759	−2.457	−2.454
103	0	90	7.987	0.141	8.175	8.721	8.166	8.154
112	0	0	−2.981	0.123	−2.834	−2.759	−2.838	−2.839
112	0	90	8.725	0.123	8.866	8.721	8.871	8.878
201	0	0	−2.804	0.143	−2.949	−2.759	−2.948	−2.946
201	0	90	8.840	0.143	9.07	8.721	9.068	9.067
004	0	0	−2.009	0.289	−2.145	−2.759	−2.145	−2.154
004	0	90	7.368	0.289	7.574	8.721	7.575	7.576
202	0	0	−2.659	0.224	−2.868	−2.759	−2.871	−2.873
202	0	90	9.272	0.224	8.926	8.721	8.931	8.938
χ^2					21.07	130.30	20.82	20.62

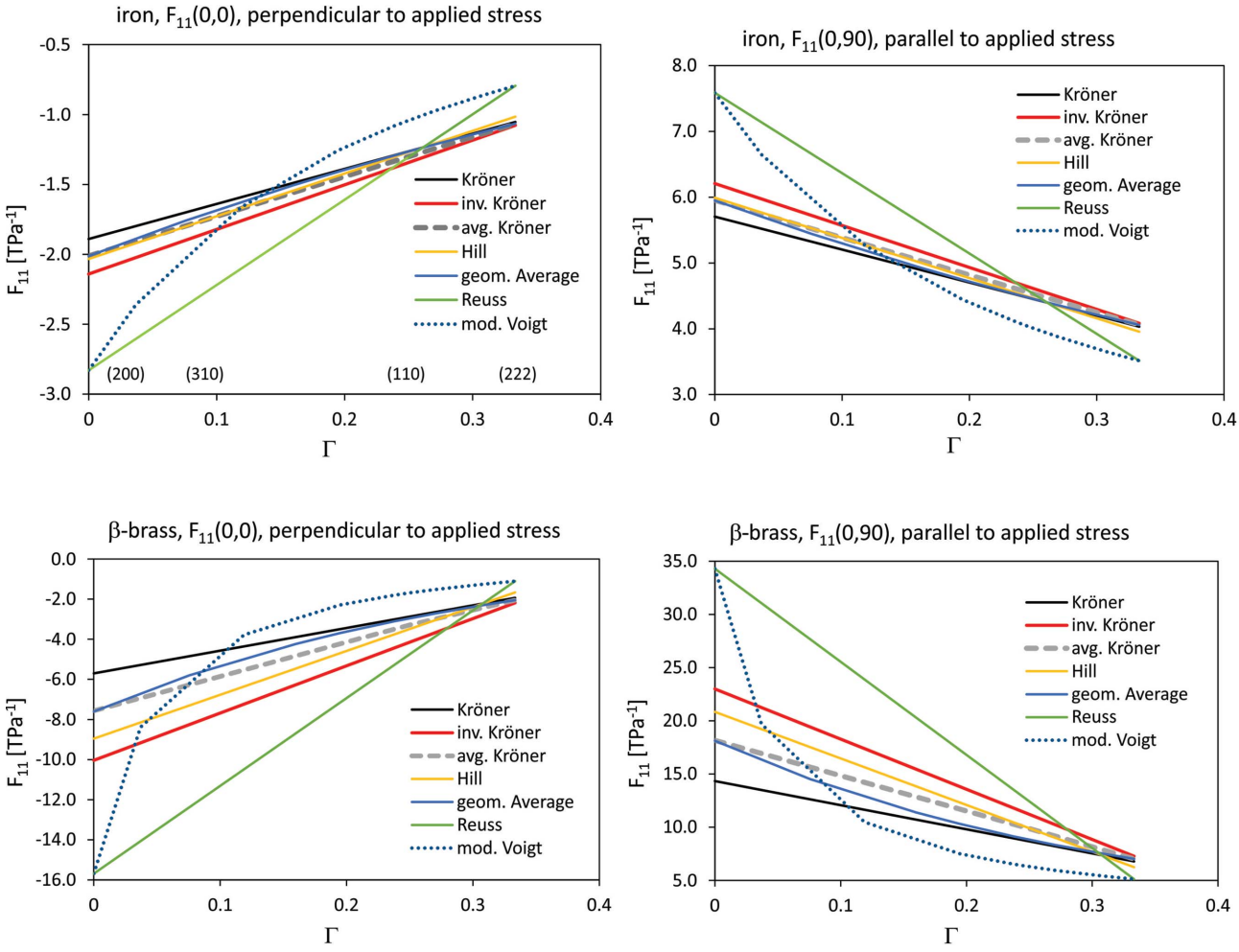

Figure 11
Isotropic (no texture) DECs for iron [single-crystal values taken from Rotter & Smith (1966)] and β-brass (Young & Bienenstock, 1971) using different models. The value of a typical uncertainty for measured DECs 1σ = 0.1 TPa^{-1} is shown. The orientation parameter on the x axis is defined as $\Gamma = (h^2k^2 + h^2l^2 + k^2l^2)/(h^2 + k^2 + l^2)^2$.

randomizations. In all cases the same outcome was found, with Reuss, Kröner-type models and Hill yielding identical results of fitted DECs, and similar results for the modified Voigt and geometric average model. The values of χ^2 for modified Voigt and the geometric average exhibit only slight differences from Reuss, Kröner-type models and Hill. Table 2 allows the conclusion that χ^2 and goodness-of-fit measures cannot be used to judge the model quality for fitting unknown SCECs. Note that fixing the overall elastic constants is equivalent to imposing constraints for Kröner-type models and the geometric average, therefore leading to a lower quality of fit.

Direct comparison with known SCECs can accomplish that; however, the differentiation of DECs from different models inside the range of achievable uncertainties is small, but it becomes larger with increasing elastic anisotropy (Fig. 11). Among the more readily available materials, copper (C11000 alloy, 99.9% pure) has the largest anisotropy. The comparison of X-ray measurements with ODF-based model calculations of $F_{11}(hkl, 0, 0)$ is shown in Fig. 12.

Fig. 12 illustrates the difficulties in evaluating model accuracy within the group of 'averaging' models (Hill, geometric

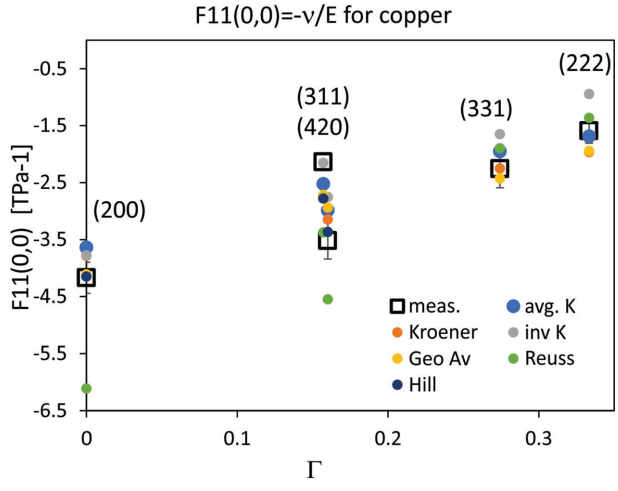

Figure 12
DECs $F_{11}(hkl, 0, 0)$ for copper from measurements and model calculations. The reflections measured are (400), (420) and (331). Lines are drawn to indicate the upper/lower bounds in the isotropic case.

Table 3
Minimum and maximum values of directional Young's modulus for various single crystals.

Values were obtained with *IsoDEC* using the Reuss model from $E = 1/F_{11}(hkl, \varphi = 0, \psi = 90^\circ)$ which delivers values for E_{hkl} identical to that of the single crystal. Single-crystal data are taken from Simmons & Wang (1971) and Young & Bienenstock (1971) for β-brass.

Material	Symmetry	$(hkl)_{min}$	$(hkl)_{max}$	E_{min} (GPa)	E_{max} (GPa)	E_{max}/E_{min}
Aluminium	Cubic	(100)	(111)	63.1	75.1	1.19
Copper	Cubic	(100)	(111)	67.4	192.2	2.85
Iron	Cubic	(100)	(111)	132.3	283.2	2.14
Nickel	Cubic	(100)	(111)	136.3	303.9	2.23
β-Brass	Cubic	(100)	(111)	29.1	194.6	6.68
Titanium	Hexagonal	(100)	(001)	104.4	143.3	1.37
α-Aluminium oxide	Trigonal	(0 33 76)	(002)	339.1	462.9	1.36
α-Uranium	Orthorhombic	(010)	(011)	148.9	287.7	1.93

average, Kröner), all of which describe the measurement results similarly well.

Most materials with an elastic range sufficiently large ($\simeq 10^{-3}$) to be suitable for DEC measurements have degrees of anisotropy that narrowly band together the Kröner-type models, the geometric average and Hill. Moreover, for cubic materials the largest differentiation between models occurs for (h00)-type reflections while DECs for high-multiplicity reflections (211) are experimentally nearly indistinguishable. For iron this range is typically covered by uncertainties of ± 0.2 TPa^{-1} or less, thus presenting difficulties for a conclusive evaluation of the mentioned models. Owing to their upper/lower bound properties, extremum values [(100)/(111) for cubic materials] obtained from Reuss, Voigt and modified Voigt are well outside experimentally established boundaries, but DECs for high-multiplicity (hkl) reflect more of the elastic behaviour of large fractions of weakly interacting grains and thus they are closer in value to the other models.

There are various definitions of elastic anisotropy in the literature (Ledbetter & Migliori, 2006; Ranganathan & Ostoja-Starzewski, 2008); however, a universal measure which is also more descriptive is introduced here as the ratio of maximum and minimum single-crystal Young's modulus. As shown in Table 3, a material with an exceptionally large elastic anisotropy such as β-brass allows distinction between models even for common high-multiplicity reflections, thus making this material a highly suitable test case for model evaluation.

It can be concluded that for materials with low anisotropy (similar to or lower than iron) the DEC models Kröner, inverse and average Kröner, Hill, and geometric average give results of similar quality with respect to goodness of fit. Fig. 12 suggests that a narrower model selection can be done once DEC data on more anisotropic materials become available. All DEC models can be used for the estimation of bulk elastic constants (Young's modulus, Poisson's ratio) which are more readily measurable; such data can be used to select DEC models on the basis of how well bulk constants agree with measurements.

3.3.2. Fitting sensitivity of SCECs with respect to (hkl) and measurement direction. A question not previously considered in the available literature on fitting SCECs (Gnäupel-Herold *et al.*, 1998; Howard & Kisi, 1999; Heldmann *et al.*, 2019; Matthies *et al.*, 2001; Wang *et al.*, 2016; Heldmann *et al.*, 2022) is whether there is an optimal strategy or DEC data set for calculating the SCECs. Such parameters include sample directions in which the F_{ij} were measured, the reflections (hkl) and whether to include overall elastic constants in the refinement. The latter can be measured without diffraction as bulk values for Young's modulus and Poisson's ratio, and such values can be used as a constraint on fits of the SCECs. The relationship between DECs, the measurement/stress direction, the reflection (hkl) and the single-crystal moduli S_{ij} can be expressed through the partial derivatives $|\mathrm{d}F/\mathrm{d}S_{ij}|$ which reflect the sensitivity of the single-crystal constants to the respective parameters.

Naturally, large sensitivities are beneficial for fitting the single-crystal constants. Fig. 13 also shows that different measurement directions are complementary and necessary in the sense that S_{ij} with $(i \neq j)$ are most sensitive to measurements perpendicular to the applied stress while S_{ii} respond best to the direction parallel to the stress direction. DEC measurements parallel to the applied stress have the advantage

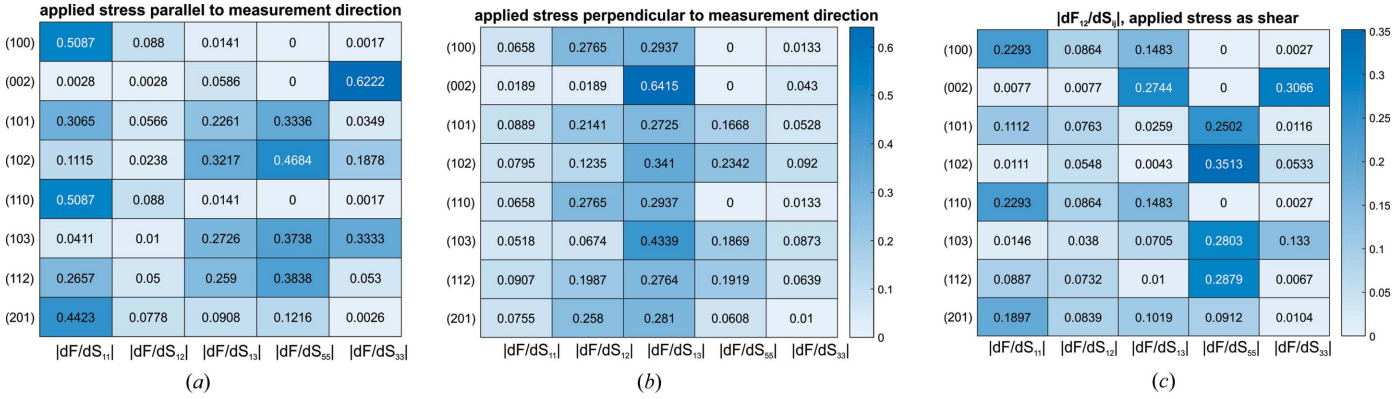

Figure 13
Sensitivities $|\mathrm{d}F(hkl)/\mathrm{d}S_{ij}|$ for titanium in the Kröner model expressed as a heatmap with (*a*) the measurement direction parallel to the direction of applied stress and (*b*) the measurement direction perpendicular to the applied stress; (*c*) the applied stress is a shear stress (σ_{12}) and F_{12} is measured in the direction ($\varphi = 45^\circ$, $\psi = 90^\circ$).

of smaller relative uncertainties because $F_{\parallel} \sim (1/\nu)|F_{\perp}|$ (ν, Poisson's ratio), meaning that $F_{\parallel}$ is larger in magnitude by a factor 3–5 while having the same uncertainties. Obtaining S_{ij} with $(i \neq j)$ benefits from measurements with mixed (hkl) and high multiplicities where the measurement direction is perpendicular to the direction of the applied stress, while for S_{ij} $(i = j)$ both directions should be parallel for maximum sensitivity $|\mathrm{d}F(hkl)/\mathrm{d}S_{ij}|$. On the other hand, measurements in shear configurations do not provide any advantages over uniaxial measurements; in contrast, sensitivities are generally lower compared with measurements with applied uniaxial stress. The condition $|\mathrm{d}F/\mathrm{d}S_{ij}| < 1$ holds for all models except the Reuss model and the modified Voigt model which are based on unbound, non-interacting grains, thus allowing $|\mathrm{d}F(hkl)/\mathrm{d}S_{ij}| = 1$ for (hkl) where the normal vector of the lattice plane is parallel to one of the Cartesian base axes of the S_{ij} [generally of the type $(h00)$, $(0k0)$ or $(00l)$].

4. Download

All calculations used in this work were performed using *IsoDEC*. *IsoDEC* can be downloaded from https://github.com/IsoDEC/IsoDEC as a zip archive.

5. Summary

IsoDEC presents a comprehensive set of methods for the calculation of elastic properties with a focus on diffraction while also including a facility for estimating overall (bulk) elastic constants. Novel approaches are the overall elastic constant calculation for multiphase aggregates with texture and non-spherical grains, a framework for fitting SCECs using measured DECs, and the calculation of DECs from EBSD data based on individual grains oriented for diffraction and the orientation of their direct neighbours. Grain-shape parameters can be utilized through the selection of suitable DEC models. The Kröner average was introduced as a new DEC model that plays the same role conceptually as the Hill average of upper and lower bounds.

Acknowledgements

The author acknowledges Dr Adam Creuziger for helpful discussions and for providing sample materials used for measuring DECs and texture.

References

Baczmanski, A., Tidu, A., Lipiński, P., Humbert, M. & Wierzbanowski, K. (2006). *Mater. Sci. Forum*, **524–525**, 235–240.
Barral, M., Lebrun, J. L., Sprauel, J. M. & Maeder, G. (1987). *Metall. Trans. A*, **18**, 1229–1238.
Behnken, H. & Hauck, V. (1986). *Z. Met.* **77**, 620–626.
Bollenrath, F., Hauk, V. & Müller, E. H. (1967). *Z. Met.* **58**, 76–82.
Brakman, C. M. (1983). *J. Appl. Cryst.* **16**, 325–340.
Bunge, H.-J. (1982). *Texture Analysis in Materials Science, Mathematical Methods*. London: Butterworths.
Creuziger, A., Hu, L., Gnäupel-Herold, T. & Rollett, A. D. (2014). *Integr. Mater. Manuf. Innov.* **3**, 1–19.
Dölle, H. (1979). *J. Appl. Cryst.* **12**, 489–501.
Eshelby, J. D. (1957). *Proc. R. Soc. London A*, **241**, 376–396.
Fisher, E. S. & Renken, C. J. (1964). *Phys. Rev.* **135**, A482–A494.
Gavazzi, A. C. & Lagoudas, D. C. (1990). *Comput. Mech.* **7**, 13–19.
Gnäupel-Herold, T., Brand, P. C. & Prask, H. J. (1998). *J. Appl. Cryst.* **31**, 929–935.
Gnäupel-Herold, T., Creuziger, A. & Iadicola, M. A. (2011). *Adv. X-ray Anal.* **55**, 128–135.
Gnäupel-Herold, T., Creuziger, A. A. & Iadicola, M. (2012). *J. Appl. Cryst.* **45**, 197–206.
Hauk, V. (1997). *Structural and Residual Stress Analysis by Nondestructive Methods*. Amsterdam: Elsevier.
Hauk, V. (1999). *Mat.-Wiss. Werkstofftech.* **30**, 377–384.
Heldmann, A., Hoelzel, M., Hofmann, M., Gan, W., Schmahl, W. W., Griesshaber, E., Hansen, T., Schell, N. & Petry, W. (2019). *J. Appl. Cryst.* **52**, 1144–1156.
Heldmann, A., Hofmann, M. & Hoelzel, M. (2022). *J. Appl. Cryst.* **55**, 656–662.
Hielscher, R. & Schaeben, H. (2008). *J. Appl. Cryst.* **41**, 1024–1037.
Hill, R. (1952). *Proc. Phys. Soc. A*, **65**, 349–354.
Howard, C. J. & Kisi, E. H. (1999). *J. Appl. Cryst.* **32**, 624–633.
Kallend, J. S., Kocks, U. F., Rollett, A. D. & Wenk, H.-R. (1991). *Mater. Sci. Eng. A*, **132**, 1–11.
Kinoshita, N. & Mura, T. (1971). *Phys. Status Solidi A*, **5**, 759–768.
Kneer, G. (1965). *Phys. Status Solidi B*, **9**, 825–838.
Kröner, E. (1958). *Z. Phys. A.* **151**, 504–518.
Ledbetter, H. & Migliori, A. (2006). *J. Appl. Phys.* **100**, 063516.
Leeuwen, M. van, Kamminga, J.-D. & Mittemeijer, E. J. (1999). *J. Appl. Phys.* **86**, 1904–1914.
Lin, S. C. & Mura, T. (1973). *Phys. Status Solidi A*, **15**, 281–285.
Matthies, S. & Humbert, M. (1995). *J. Appl. Cryst.* **28**, 254–266.
Matthies, S., Priesmeyer, H. G. & Daymond, M. R. (2001). *J. Appl. Cryst.* **34**, 585–601.
Möller, H. & Martin, G. (1939). *Mitt. Des. Kaiser-Wilhelm-Inst. Eisenforsch.* **21**, 261–269.
Morris, P. R. (1970). *Int. J. Eng. Sci.* **8**, 49–61.
Mura, T. (1987). *Micromechanics of Defects in Solids*. Dordrecht: Springer Netherlands.
Murray, C. E. & Noyan, I. C. (1999). *Philos. Mag. A*, **79**, 371–389.
Pal, S., Bhanuprasad, V. V., Mitra, R. & Ray, K. K. (2009). *Metall. Mater. Trans. A*, **40**, 3171–3185.
Ranganathan, S. I. & Ostoja-Starzewski, M. (2008). *Phys. Rev. Lett.* **101**, 055504.
Reuss, A. (1929). *Z. Angew. Math. Mech.* **9**, 49–58.
Rotter, C. A. & Smith, C. S. (1966). *J. Phys. Chem. Solids*, **27**, 267–276.
Sato, A., Mori, T. & Tanaka, Y. (1979). *Acta Metall.* **27**, 131–136.
Simmons, G. & Wang, H. (1971). *Single Crystal Elastic Constants and Calculated Aggregate Properties*. Cambridge: The MIT Press.
Suryanarayana, C. (2011). *J. Alloys Compd.* **509**, S229–S234.
Voigt, W. (1928). *Lehrbuch der kristallphysik (mit ausschluss der kristalloptik)*. Leipzig, Berlin: B. G. Teuber.
Walpole, L. J. (1969). *J. Mech. Phys. Solids*, **17**, 235–251.
Wang, Z., Stoica, A. D., Ma, D. & Beese, A. M. (2016). *Mater. Sci. Eng. A*, **674**, 406–412.
Willis, J. R. (1977). *J. Mech. Phys. Solids*, **25**, 185–202.
Wit, R. de (1997). *J. Appl. Cryst.* **30**, 510–511.
Young, P. L. & Bienenstock, A. (1971). *J. Appl. Phys.* **42**, 3008–3009.